OPEN JOURNAL SYSTEMS
ISSN: 2595-4431

Brazilian **J**ournal of **E**nvironment, v.9, n.3. 048-062 (2021)

Brazilian Journal of Environment

Alves et al

Revista Brasileira de Meio Ambiente

Spatiotemporal geostatistics applied to surface albedo: The case of southern Minas Gerais (Brazil)

Henrique José de Paula Alves[1]*, Luana Mendes dos Santos[2], Ben Dêivide de Oliveira Batista[3]

[1]*Researcher, Institute for Applied Economic Research, Rio de Janeiro, RJ, Brazil (*Corresponding author: henrique.alves@ipea.gov.br)*
[2]*PhD student in Agricultural Engineering, Substitute Professor, Federal University of Itajubá, Brazil.*
[3]*Professor, Federal University of São João del Rei, Brazil.*

History: Submitted: 11/07/2021 - Revised: 30/07/2021 - Accepted: 01/09/2021

A B S T R A C T

Several science areas have data coming characterized by variations in space and time that are measured using statistical procedures that take into account or not the existing interactions between the dimensions of space and time. Gneiting, in 2002, proposed a model that is based on the construction of non-separable stationary covariance functions, given the condition of being positive definite, which can be used to model the covariance matrix used in kriging. The southern mesoregion of Minas Gerais is very important to Brazilian agribusiness due to the planting of coffee cultivar and also because it has an extensive pasture area, allowing the creation of cattle, horses, and pigs and, for this reason, it is essential to study factors that impact on the climate of this region as the Earth's surface albedo, which is defined as the ability of a surface to reflect solar radiation. This article's objective is to apply the covariance model presented by Gneiting to the Geostatistical modeling of a set of real data on the albedo of the Earth's surface in the mesoregion in question using ordinary kriging to predict data of this nature. We choose to use the linear kriging predictor as it has the property of being best linear unbiased prediction (BLUP). We conclude that the exponential-cauchy family belonging to the class of covariance functions presented by Gneiting obtained a lower MSE in the adjustment of the covariance matrix of the linear kriging predictor and, therefore, can be used to predict the Earth's surface albedo.

Keywords: Albedo, space-time, covariance, Gneiting

Modelagem geoestatística espaço-temporal de Gneiting aplicada ao albedo de superfície

R E S U M O

Diversas áreas da ciência possuem dados vindos caracterizados por variações no espaço e no tempo que são medidos por meio de procedimentos estatísticos que levam em consideração ou não as interações existentes entre as dimensões do espaço e do tempo. Gneiting, em 2002, propôs um modelo que se baseia na construção de funções de covariância estacionárias não separáveis, na condição de serem de definidas positivas, que podem ser utilizadas para modelar a matriz de covariâncias utilizada na krigagem. A mesorregião sul de Minas Gerais e muito importante para o agronegócio brasileiro devido ao plantio da cultivar de café e também por possuir uma extensa área de pastagem, permitindo a criação de bovinos, equinos e suínos e, por isso, é imprescindível o estudo. fatores que impactam o clima dessa região como o albedo da superfície terrestre, que é definido como a capacidade de uma superfície refletir a radiação solar. O objetivo deste artigo e aplicar o modelo de covariância apresentado por Gneiting a modelagem geoestatística de um conjunto de dados reais sobre o albedo da superfície terrestre na mesorregião em questão usando krigagem ordinária para predizer dados dessa natureza. preditor de krigagem, pois tem a propriedade de ser a melhor predição linear não enviesada (BLUP). Concluímos que a família exponencial-cauchy pertencente a classe de funções de covariância apresentada por Geniting obteve um MSE inferior no ajuste da matriz de covariância do preditor de krigagem linear e, portanto, pode ser usada para prever o albedo da superfície da Terra.

Palavras-Chaves: albedo, espaco-tempo, covariância, Gneiting

Alves, H. J. P., dos Santos, L. M.., Batista, B. D. O. (2021). Spatiotemporal geostatistics applied to surface albedo: The case of southern Minas Gerais (Brazil). **Brazilian Journal of Environment**, v.9, n.3, p.48-62.

1. Introdução

The Earth's surface albedo, defined as the global fraction of solar radiation reflected by the Earth's surface (Gueymard, 1993), is a key component in the modeling of various agronomic, physiological, biological, and biogeochemical processes (Yin, 1998; Iziomon and Mayer, 2002; Psiloglou and Kambezidis, 2009; Zhang et al., 2013), and, in general, due to economic, and technical aspects, it is observed in different seasons (Iqbal, 2012). Due to the spatio-temporal variation associated with each Earth's surface's properties and external factors, the Earth's surface albedo obtained by measurements at specific locations is generally not applicable to other unmonitored locations it is customary to use a constant value as a standard alternative, that is, 0.20 for a vegetation-free and snow-free surface (Jordan, 1963) and 0.23 for areas with vegetation cover of some hypothetical crop (Allen et al., 1998).

However, numerous land, aerial, and even satellite measurements have shown that Earth's surface albedo undergoes wide regional, and latitudinal variations (Iqbal, 2012; Maghrabi and Al-Mostafa, 2009). Consequently, the use of an invariable standard value of the Earth's surface albedo results in great uncertainties in the estimated radiation, and, therefore, generates several other radiation-dependent parameters such as surface temperature, evaporation, and evapotranspiration. This fact makes the derivation of timely and accurate estimates of the Earth's surface albedo with spatio-temporal variations increasingly important in many aspects. Many researchers have been concerned about this as can be seen in Zolotokrylin, Brito-Castillo and Titkova (2020); Zhou et al. (2020); Wang et al. (2020); Li, Zhang and Qu (2020); Liao et al. (2020). However, research aimed at Brazil is still incipient and necessary, given the importance of Brazilian agribusiness studies.

As already mentioned, the spatio-temporal variation of the Earth's surface albedo and the absence of accurate estimates substantially impact several other radiation-dependent parameters. In this sense, Liao et al. (2020) were concerned to characterize the Earth's surface albedo in the interior of Tibetan Plateau (China) since it is a region that snows a lot. Meng (2020) also studied the spatio-temporal variation of the Earth's surface albedo in Beijing, China, as it is a very urbanized region and, consequently, with a lot of solar irradiation reflectance (albedo). Lin et al. (2020) analyzed the temporal space variability of the Earth's surface albedo in Tibetan Plateau, China, between 2001 and 2019, associating the correlations between the anomalies existing in the Earth's surface albedo and the anomalies of different types of vegetation. Zolotokrylin et al. (2020) related the effects of Earth's surface albedo and Earth's surface temperature values in Sonora, Mexico.

Data that are characterized by variations present in space and time come from spatiotemporal processes, and the purpose of statistical analysis for this type of data is not only to describe the uncertainty about the estimates of the attribute of interest, but also to estimate values in places not sampled. Gneiting (2002) proposes a class of stationary non-separable covariance functions to model the spatiotemporal covariance matrix present in the linear kriging predictor.

In this context, the modeling proposed by Gneiting (2002) was applied to albedo data of the Earth's surface in the southern mesoregion of Minas Gerais, located in Brazil, which is very rich in products from agribusiness, with coffee growing as its main products. , corn and soybeans (Garcia, Mattoso and Duarte, 2006; Reis et al., 2001; Silva, Santos and Lima, 2001; Carvalho et al., 2010; Silva and Maciel, 2010; Rodrigues et al. 2009).

The objective of this work is to predict the Earth's surface albedo in this mesoregion on the 31st of December of the year 2019 using geostatistical spatiotemporal modeling. The motivation for using the linear kriging predictor is because it has the property of being the best linear unbiased predictor (BLUP) (Cressie, 1990), in addition to surface albedo estimates using predictors with smaller errors, it has the importance to highlight environmental imbalances (Lima et al., 2021), and to contribute to identify urban heat islands due to areas with exposed soil as evidenced by Silva, Loureiro and Sousa (2021).

2. Material e Métodos

2.1 Earth surface albedo

According to Bonn (2008), the albedo of the earth's surface (A) is the ratio between the radiation reflected by the earth's surface ($F_{s\omega\uparrow}$) and the radiation incident on it ($F_{s\omega\downarrow}$). Its expression is given by equation 1:

$$A = \frac{F_{s\omega\uparrow}}{F_{s\omega\downarrow}} \quad (1)$$

It is an dimensionless measure, and for this reason, it is expressed in terms of percent with values between 0 and 1, not being a property of the Earth's surface but a characteristic of the Earth-atmosphere Bonn (2008) system. It is also one of the most important variables on the Earth's surface that a effects Earth's climate (Dickinson, 1983; Sarafanov, 2020). The value 0 represents no reflection (black earth surface) and the value 1 represents total reflection (white earth surface). It brings some important effects to the ecosystem such as effects on heatstroke, e effects on climate, e effects on albedo-temperature feedback, e effects on snow formation, small- scale e effects (feeling of heat and freshness by wearing dark and light clothes), effects on reforestation of trees (photosynthesis) reducing deforestation of trees, e effects on water, e effects on cloud formation Bonn (2008).

2.2 The linear predictor of space-time kriging

Suppose that n locations S_1, S_2, ..., S_n are sampled and at each location there is a time series at T different times. Then, the set of observations, or spacetime random field, $Z(S_i; T_j)$, i = 1,2,,..,n; j= 1, 2, ..., T, where Z(.) is the response variable of interest. The main objective is to build a model that can make predictions for unsampled S_i locations at a specific time T_j.

Consider a spatiotemporal random field $Z(S_i; T_j)$. The technique known as kriging is a regression method used in geostatistics to approximate or interpolate data. Kriging is often the ultimate goal in random field analysis, and the validity of the prediction is influenced by specifying the covariance function or theoretical semivariogram models (Stein, 2012). The correct estimation of the parameters of these models is also of paramount importance.

Consider $Z(S_0; T_0)$ an unobserved value of some attribute Z located in space and time, respectively, where S_0 is the spatial location and T_0 is the location in time. The linear spacetime kriging predictor has the following properties: it is unbiased and has minimal variance. For the case where μ(S; t) is known and constant, we have the predictor known as ordinary kriging.

2.3 Ordinary kriging variance (prediction error)

The variation of the estimate quantifies the error value when evaluating Z(S0; t0) using Z ̂(S0; t0). The kriging variance is a particular case of the estimate variance, being its smallest value.

Sampling is usually done at a set of points sparsely distributed throughout the study area, and the aim is to describe the random field continuously throughout the area. However, to predict random spacetime fields, obtaining theoretical semivariogram models can be very complicated. A more direct way is to consider theoretical models of stationary covariance functions as presented by Gneiting (2002).

2.4 Gneiting's class of covariance functions

Gneiting (2002) considers two possible forms of modeling for data coming from a spatio-temporal structure: a geostatistical specification and another based on models. The geostatistical specification, which will be considered in this paper, generally uses kriging, and the vector of averages is easily specified by the context, which does not occur with the covariance matrix, whose elements are given by a valid covariance function in which the defined positive condition is ensured. The modeling of this matrix covariance root is the key point of this article and, therefore, gneiting2002 presents a model given by the equation 4:

$$W = \sum(\boldsymbol{h}, u) = \frac{\sigma^2}{(\psi|u|^2)^{d/2}} \emptyset\left(\frac{\|\boldsymbol{h}\|^2}{\psi|u|^2}\right), \quad (\boldsymbol{h}, u) \in \mathbb{R}^d \times \mathbb{R} \qquad (4)$$

where $\|.\|$ is the Euclidean quadratic norm between two georeferenced locations in space and separated by a Euclidean spatial distance $\mathbf{h} = \|\boldsymbol{S}_i - \boldsymbol{S}_j\|$, $|u| = |t_i - t_j|$ is the time shift where $|.|$ represents the module, σ^2 is the variability of the random field. Specifically, $\phi(t)$, $t \geq 0$, is any completely monotone function and $\psi(t)$, $t \geq 0$, is any positive function with a completely monotone derivative. Gneiting (2002) presents two classes of functions that meet the condition of $\phi(t)$ and $\psi(t)$. Each covariance function model is obtained by replacing the possible combinations of these functions in the expression ref geniting model. Some of these combinations generate families of known models, such as models of the exponential class and the Whittle Matérn family.

Table 1 – Completely monotone functions.

Functions ($\phi(t)$)	**Parameters**
$e^{-ct^{\gamma}}$	$c \geq 0, 0 < \gamma \leq 1$
$(2^{\upsilon-1}(\upsilon))^{-1}(ct^{1/2}K_{\upsilon}(ct^{1/2})$	$c > 0, \nu > 0$
$(1 + ct^{\gamma})^{\upsilon}$	$c \geq 0, 0 < \gamma \leq 1, \nu > 0$
$2^{\upsilon}(e^{(ct^{1/2})}) + e^{(ct^{1/2})})^{\upsilon}$	$c > 0, \nu > 0$

Source: From the author (2021)

Table 2 – Positive functions with a completely monotone derivative.

Functions ($\boldsymbol{\psi}(\boldsymbol{t})$)	**Parameters**
$e^{-ct^{\gamma}}$	a > 0,0 α ≤ 1, 0 ≤ β ≤ 1
$2^{\upsilon-1}(\upsilon))^{-1}(ct^{1/2}K_{\upsilon}(ct^{1/2})$	a > 0, b > 1, 0 ≤ α ≤ 1
$2^{\upsilon}(e^{(ct^{1/2})}) + e^{(ct^{1/2})})^{\upsilon}$	a > 0,0 < b ≤ 1, 0 <α ≤ 1

Source: From the author (2021)

2.5 Study area

The albedo variable data is located in the southern mesoregion of Minas Gerais, in Brazil, and this collection was performed by satellite image processing. Images from the series of geostationary satellites

METEOSAT 9 from the European Organization for the Exploitation of Meteorological Satellites (EUMETSAT) were used.

This satellite has instruments such as GERB radiometer (Geostationary Earth Radiation Budget), communication instruments such as GEOS & R (Geostationary Search and Rescue), DCS data storage platform (Data Collection System), and the SEVIRI sensor (Spinning Enhanced Visible and Infrared Imager). This SEVIRI sensor is equipped with 12 spectral channels, ranging from visible wavelengths to distant infrared wavelengths, including bands of water vapor, ozone, and carbon dioxide absorption, with a spatial resolution between 1 km to 3 km in Nadir (Fensholt et al., 2006).

The temporal resolution is capable of obtaining meteorological images every 15 minutes in nominal mode or 5 minutes in fast mode. In this way, the values obtained every 15 minutes on METEOSAT-9 can be acquired 96 times a day.

The albedo variable of the Earth's surface was considered, collected in a daily average of each of the 31 days of December of the year 2019, so that the observations for the calculation of the standard were obtained every 15 minutes in the period between 08:00 am and 5:00 pm, totaling 36 observations at each location. The samples for analysis are arranged in a mesh with 500 spatial locations, the same locations being considered on each evaluated day.

The study region is a mesoregion with a high concentration of coffee plantations and many pasture areas, providing cattle, horses and swine. Therefore, it is interesting to present some characteristics of this mesoregion, such as location, surface temperature, evapotranspiration, relative humidity, precipitation and vegetation. Figure 1 shows these characteristics of the southern mesoregion of Minas Gerais, located in Brazil. It is observed in Figure 1 (b) that it is a mesoregion whose temperature is high (22 ºC) in the north and, as it moves to the south, the temperature drops (8.5 ºC) causing the south of this region. mesoregion is a cooler area. In Figure 1 (c), it is also noted that the evapotranspiration of this mesoregion varies from medium (north and northeast) to high (south and southeast), with rare exceptions for places with low evapotranspiration. The opposite is true for the relative humidity of the air (Figure 1 (d)). Figures 1 (e) and 1 (f) show the precipitation and vegetation of this mesoregion. It is noted that the places of high precipitation are concentrated further south of this mesoregion (Figure 1 (e)), and it is noted that it is a mesoregion with rivers, a high concentration of forests, eucalyptus and pine trees, and the highest concentration of urbanized area occurs to the south of this mesoregion (Figure 1 (f)).

Figure 1 – Characterization of the southern region of Minas Gerais in Brazil: location, surface temperature, evapotranspiration, relative humidity, precipitation and vegetation.

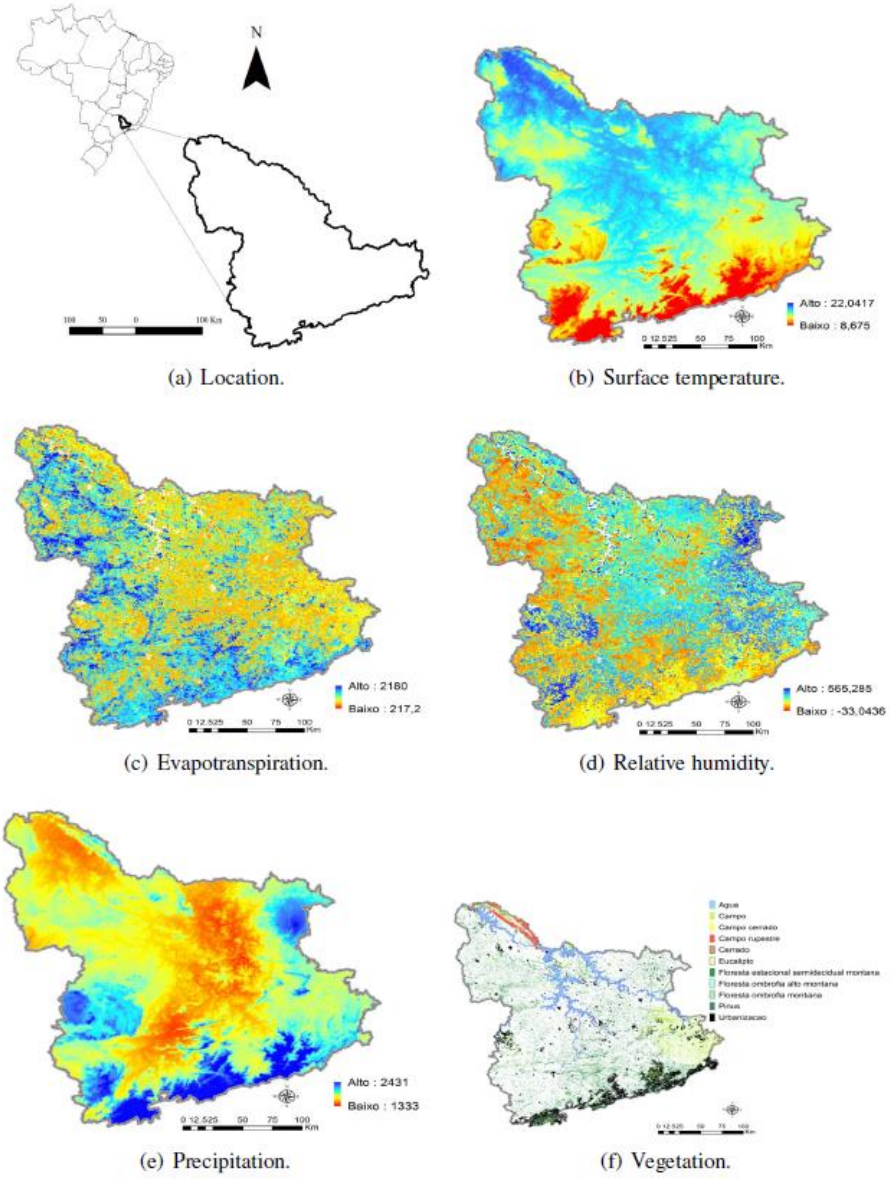

(a) Location. (b) Surface temperature. (c) Evapotranspiration. (d) Relative humidity. (e) Precipitation. (f) Vegetation.

Source: From the author (2021)

In general, the adjustment of models in any statistical analysis should only be carried out if the collected observations do not present any trend (stationarity). The geostatistical study is no different. We then performed the average stationarity test Kwiatkowski–Phillips–Schmidt–Shin (KPSS) as in KQBŁ Owski and Welfe (2004) in order to verify that the albedo data are stationary (Table 3), whose null hypothesis H0 implies data stationarity. So, we believe we have evidence that the data are stationary and therefore, the use of the model proposed by Gneiting (2002), as in equation 5 is adequate. With this information, we then adjusted the covariance function model as in the section 2.4.

Table 3 – Trend test measures KPSS. Here KPSS trend is the value of the test statistic, p-value is the p-value associated with the test statistic, and Decision is the decision made based on the p-value obtained.

KPSS Trend	p-value	Decision
0.13266	0.07469	No rejection H0

Source: From the author (2021)

3.1 The adjusted Gneiting model

All possible combinations of functions displayed by Gneiting (2002) (see Tables 1 and 2) and chose that combination with the lowest Mean Square Error (MSE). The lowest MSE (0.000018) was obtained by combining the first entry in Table 1 with the second entry in Table 2 (exponential-cauchy family) and, therefore, the model considered is presented in the expression 3:

$$W = \sum(\boldsymbol{h}, u) = \frac{\sigma^2}{(a|u|^{2\alpha}+1)^{\beta d/_2}} exp\left(-c\frac{\|\boldsymbol{h}\|^{2\gamma}}{(a|u|^{2\alpha}+1)^{\beta\gamma}}\right), \in \mathbb{R}^d \times \mathbb{R} \quad (3)$$

$$C_0(\mathbf{h}=0,u) = \frac{\sigma^2}{(a|u|^{2\alpha}+1)^{\beta d/_2}} \quad (4)$$

The nugget e effect equation 4 is obtained by taking h = 0 to equation 3, and is de ned as an uncontrollable sampling error. The quantities a and α are the scaling and smoothness parameters of the process over time, respectively, γ is the smoothness parameter of the process in space, β is the parameter that measures the strength of the interaction between space and time and d is the dimension of space. Considered the two-dimensional space (d = 2) to obtain the parameter estimates for the model presented in the expression equation 3. Table 4 presents the estimates of the Gneiting model's parameters as in equation 3.

Table 4 – Estimates of the parameters of the considered covariance function model: σ^2 is the random field variance, γ is the n space smoothness parameter, α is the time smoothness parameter, c is the space scale parameter, a is the time scale parameter, β is the parameter that measures the strength of interaction between space and time, $\boldsymbol{C_0}\,(\boldsymbol{h}=\boldsymbol{0},\boldsymbol{u})$ is the nugget effect, d = 2 is the dimension of space.

$\boldsymbol{\sigma^2}$	$\boldsymbol{\gamma}$	$\boldsymbol{\alpha}$	**c**	$\boldsymbol{a}$	$\boldsymbol{\beta}$	$\boldsymbol{C_0}\,(\boldsymbol{h}=\boldsymbol{0},\boldsymbol{u})$
4.298×10^{-16}	1.03×10^{3}	3.17×10^{2}	4.47×10^{3}	1.79×10^{1}	1.00×10	3.14×10^{-1}

Then, the adjusted model of covariance functions and nugget effect, as in equation 5 and equation 6, is presented in the following expression:

$$W = \frac{4.298 \times 10^{-16}}{(1.79 \times 10|u|^{6.34 \times 10^2}+1)} exp\left(-4.47 \times 10^3 \frac{\|\boldsymbol{h}\|^{2.06 \times 10^3}}{(3.17 \times 10^2|u|^{6.34 \times 10^2}+1)^{3.17 \times 10^2}}\right) (5)$$

$$C_0(\mathbf{h}=0,u) = 3.14 \times 10^{-1} \quad (6)$$

Figure 2 shows the sample and adjusted covariograms for the model presented in the section 2.4.

Figure 2 – Sample and adjust covariogram for the Gneiting model.

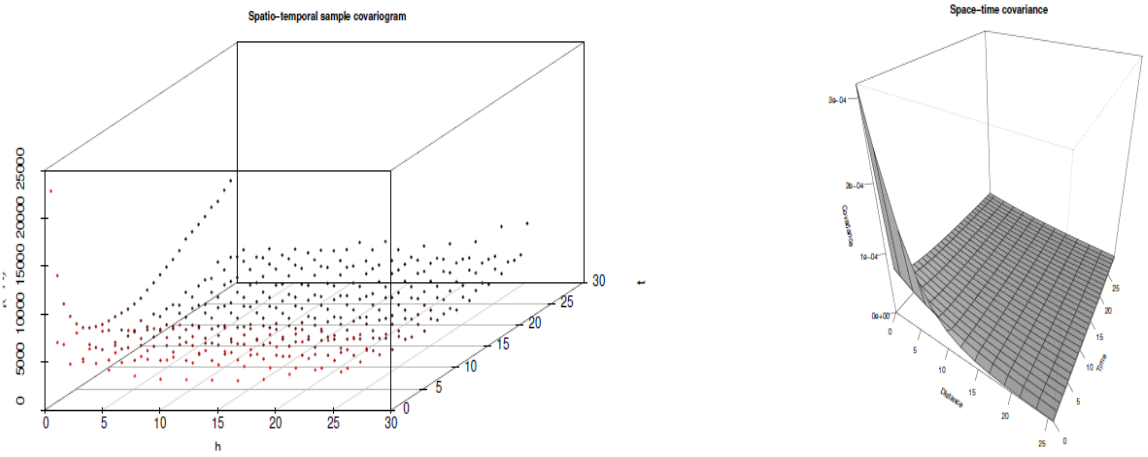

(a) Sample covariogram. (b) Adjusted covariogram.

Source: From the author (2021)

3 Results and Discussion

3.1 Spatio-temporal kriging maps

In Figure 3, the average Earth's surface albedo in this mesoregion suffered variations in concentration over the considered days. We note in Figure 3 (a) that the highest average concentration of the Earth's surface albedo (0.20) is located in the south-central and also southwest of this mesoregion. The average found for the grazing areas in Figure 3 (a) was 0.16, this value is in line with those of giongo2009 from 0.14 to 0.16, and within the range of surface albedo presented by campos2020 from 0.15 to 0.25 in areas of undergrowth, including pastures and agricultural areas and also according to the studies by campos2020 in which the albedo in the pasture areas were within the range of 0.145 to 0.156. For the agricultural areas in Figure 3 (a) an albedo average of 0.16 was also found. This result shows little variation in the values when compared to other agricultural areas that can vary from 0.13 to 0.19 (Giongo et al., 2009). On the fourth day (Date 4), the largest concentration of albedo moves to this mesoregion's central area. A curious fact is that in these areas of greater concentration of the Earth's surface albedo are the areas of low surface temperature (Figure 1 (b)), except the fourth day (Date 4) that is found in the central area and whose surface temperature is high (Figure 1 (b)). In addition, it is an area of greater concentration of the Earth's surface albedo with low evapotranspiration (Figure 1 (c)), high relative humidity (Figure 1 (d)), high precipitation (Figure 1 (e)) with the exception of the fourth day (Date 4) which has low precipitation. About vegetation and urbanized area, the high concentration of albedo on Earth's surface is located in areas of concentration of forest, eucalyptus and also of little urbanization (Figure (f)).

We also notice in Figures 3 (b), 3 (c), 3 (d), 3 (e) and 3 (f) that the highest concentration of Earth's surface albedo remains in the center-south and southeast of the southern mesoregion of Minas Gerais (0.22). A curious fact is that on the eighth day (Date 8), in almost the entire area of this mesoregion, the Earth's surface albedo had an average value of around 0.14. As the data were obtained via a satellite image, it may be that there was heavy rain or even a high presence of clouds in practically the entire region that day. Clouds and heavy rains act as a barrier to obtain satellite images Geiger (2008).

Figure 3– Kriging maps of the daily average of the Earth's surface albedo in the 31 days of December of the year 2019.

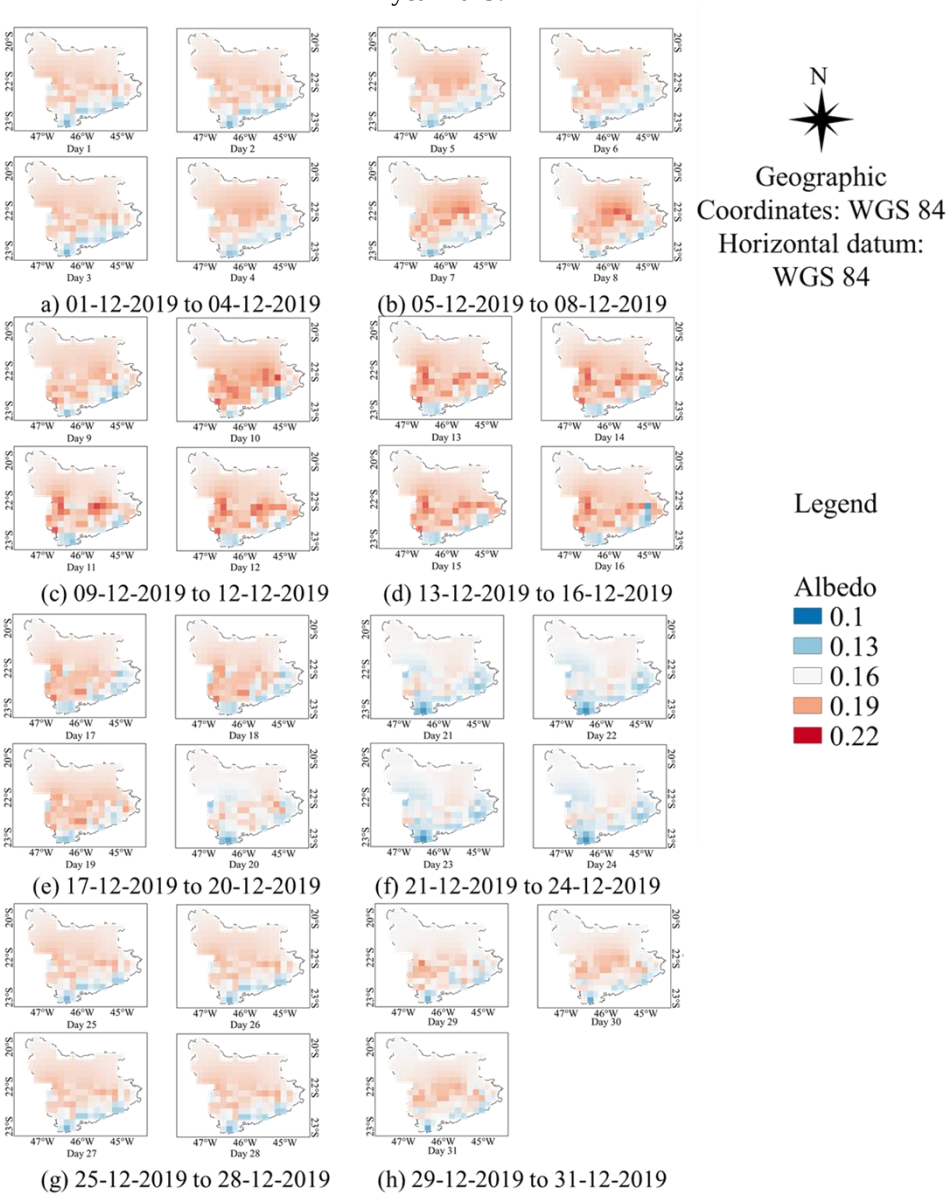

Source: From the author (2021)

Specifically, Ridgwell (2009) suggest that the existing global infrastructure is associated with arable agriculture, given that crop plants exert an important in influence over the climatic energy budget because of differences in their surface albedo compared to soils and natural vegetation. Rhland (2019) studied of decomposition of plant litter exposed to solar radiation, where one factor that may influence incident solar radiation is surface albedo. The authors examined the influence of different surface albedos on the photodegradation in southern Minnesota. Doughty (2011) evaluated the Earth's surface to increase albedo and test whether increasing agricultural albedo can cool regional climate. Still, Irvine (2011) present results of a

series of atmosphere-ocean general circulation model (GCM) simulations to compare three surface albedo geoengineering proposals: urban, cropland, and desert albedo enhancement. Liu (2020) quantify the significance of deforestation's biophysical effects through studies of the Earth's surface albedo. lone2020 evaluated the influence of climate change and Earth's surface albedo on vegetation. This is an important parameter, varying according to changes in land use and cover and soil conditions and humidity (Oliveira et al., 2015), directly impacting the energy balance and climate.

In addition, understanding albedo behavior improves our understanding of vegetation phenology during land-atmosphere interactions (Wang et al., 2018). Darker areas such as grasses, plantations, soil treatment for planting (color change), among other factors such as the presence of clouds, are possible indicators of the lower albedo of the earth's surface.

This characteristic occurs because the lower the albedo, the higher the evapotranspiration rates, which leads to the conclusion that significant changes in albedo patterns caused by changes in land use can alter evaporation and transpiration patterns, such as the replacement of arboreal vegetation by agricultural areas or pastures. Thus, this change directly impacts irrigation management in agricultural areas and, therefore, according to the conclusion of the studies by Campos, Adami and Araújo (2020), the albedo estimate is useful to create strategies that provide subsidies in the implementation of instruments management and agricultural and environmental planning in view of the expansion of crops. In general, it is noted in Figure 3 that the albedo value in the southern mesoregion of Minas Gerais is concentrated between 0.10 and 0.22 for the 31 days of December 2019.

Future studies on the albedo responses of the study region are recommended, analyzing the months of the year to associate the seasons of the year and their behavior in different years for the analysis of climatic variations due to changes in land use.

3.2 Spatio-temporal kriging maps of variance

The fit quality of the linear kriging predictor used (see section 2.2) together with the covariance function model used (see section 2.4) is measured using the kriging variance (see section 2.3). Figure 4 shows the kriging variance maps for the average daily variation of the Earth's surface albedo measured over the 31 days of December 2019. In general, we note that the linear kriging predictor used described the behavior of the Earth's surface albedo in the southern mesoregion of Minas Gerais satisfactorily, with a prediction error of at most 0.02.

Figure 4– Kriging standard deviation maps of the daily mean of the Earth's surface albedo in the 31 days of December of the year 2019.

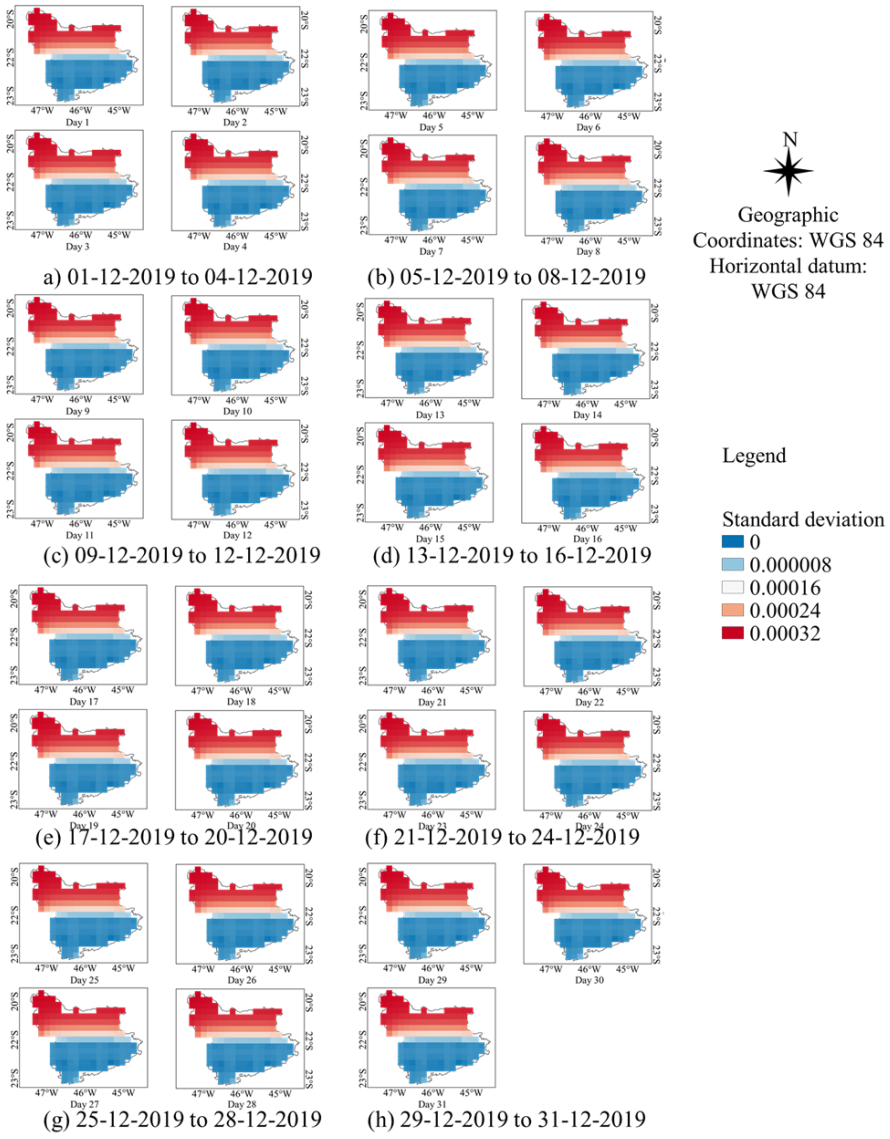

Source: From the author (2021)

In general, it is noted that the linear kriging predictor used described the behavior of the Earth's surface albedo in the southern mesoregion of Minas Gerais in a satisfactory manner, with a maximum prediction error of 0.02. This result shows the characteristic of the linear kriging predictor to be the best unbiased predictor, making it possible to obtain estimates of the surface albedo in the entire study area and especially in places that were not sampled with the smallest possible error of variance.

The authors Lima et al. (2021), studying the behavior of albedo in the city of Petrolina, applied satellite image classification to generate specialized surface albedo data, for accuracy analysis and to measure the performance of the classifier used, the authors used the Kappa Index , a measure from 0 to 1 that reverberates how far the observations are from the expected observations, it is noteworthy that the authors obtained a kappa

index of 0.61, which is considered a very good classification accuracy. In this study, a totally different and unprecedented approach was used for albedo estimates, as they are different approaches, it is not possible to be compared, however, Figure 4 reverberates that the standard deviation of kriging for the daily mean of albedo was the same for all days studied in addition to being a variation very close to zero, being a reliable methodology for the spatialization of environmental variables.

4. Conclusion

It was possible to apply the spatiotemporal modeling using geostatistics using covariance functions. The proposal considered in this work proved to be useful to model the land surface albedo observed on December 31, 2019 in the southern mesoregion of Minas Gerais, located in Brazil, due to obtaining the minimum kriging variance, with prediction errors close to zero.

There were daily variations, being possible to observe these variations along the studied days, mainly due to precipitation and the presence of clouds. It was observed that the high concentration of surface albedo in the study area is located in areas with a concentration of forest, eucalyptus and also with little urbanization.

5. References

Allen, R.G., Pereira, L.S., Raes, D., & Smith, M., (1998). Crop evapotranspiration-guidelines for computing crop water requirements-FAO irrigation and drainage paper 56. **Fao, Rome**, 300, D05109.

Campos, M. S.; Adami, M.; & Araújo, A. C., (2020). Análise do Albedo de Superfície da Palma de óleo e Diferentes Usos e Coberturas do Solo no Leste da Amazônia. **Revista Brasileira de Meteorologia**, 36, 15-21.

Carvalho, E. R., Rezende, P. M. D., Ogoshi, F. G. A., Botrel, É. P., Alcantara, H. P. D., & Santos, J. P., (2010). Desempenho de cultivares de soja [Glycine max (L.) Merri] em cultivo de verão no sul de minas gerais. **Ciência e Agrotecnologia,** 34, 892–899.

Cressie, N., (1990). The origins of kriging. **Mathematical geology**, 22, 239–252.

Dickinson, R. E., (1983). Land surface processes and climate—surface albedos and energy balance. **Advances in geophysics**. Elsevier, 25, 305–353.

Doughty, C. E., Field, C. B., McMillan, & A. M., (2011). Can crop albedo be increased through the modification of leaf trichomes, and could this cool regional climate? **Climatic Change**, 104(2), 379–387.

Fensholt, R., Sandholt, I., Stisen, S., & Tucker, C., (2006). Analysing NDVI for the African continent using the geostationary meteosat second generation SEVIRI sensor. **Remote Sensing of Environment**, 101, 212–229.

Garcia, J. C., Mattoso, M. J., DUARTE, & J. de O., (2006). Importância do milho em Minas Gerais. **Embrapa Milho e Sorgo - Artigo em periódico indexado (ALICE)**.

Geiger, B., Carrer, D., Franchisteguy, L., Roujean, J.L., & Meurey, C., (2008). Land surface albedo derived on a daily basis from Meteosat Second Generation observations. **IEEE Transactions on Geoscience and Remote Sensing**, 46(11), 3841–3856.

Giongo, P. R.; Padovani, C. R.; & Vettorazzi, C. A., (2009). Variabilidade espacial e temporal do albedo obtido a partir de imagens MODIS na região do Pantanal. **Anais 14° Simpósio Brasileiro De Sensoriamento Remoto**, 14, 4715-4722.

Gneiting, T., (2002). Nonseparable, stationary covariance functions for space–time data. **Journal of the American Statistical Association**, 97, 590–600.

Gueymard, C., (1993). Critical analysis and performance assessment of clear sky solar irradiance models using theoretical and measured data. **Solar Energy**, 51, 121–138.

Iqbal, M., (2012). **An introduction to solar radiation**. Elsevier.

Irvine, P. J., Ridgwell, A., & Lunt, D. J., (2011). Climatic effects of surface albedo geoengineering. **Journal of Geophysical Research: Atmospheres**, 116(D24).

Iziomon, M., Mayer, & H., (2002). On the variability and modelling of surface albedo and long-wave radiation components. **Agricultural and Forest Meteorology**, 111, 141–152.

Jordan, R., (1963). The long-term average performance of flat-plate solar energy collectors. **Solar Energy**, 7, 53–74.

Kqbłowski, P., & Welfe, A., (2004). The ADF-KPSS test of the joint confirmation hypothesis of unit autoregressive root. **Economics Letters**, 85, 257–263.

Li, X., Zhang, H., & Qu, Y., (2020). Land surface albedo variations in SanJiang plain from 1982 to 2015: Assessing with glass data. **Chinese Geographical Science**, 30(5), 876–888.

Liao, W., Liu, X., Burakowski, E., Wang, D., Wang, L., & Li, D., (2020). Sensitivities and responses of land surface temperature to deforestation-induced biophysical changes in two global earth system models. **Journal of Climate**, 33(19), 8381–8399.

Lin, X., Wen, J., Liu, Q., You, D., Wu, S., Hao, D., Xiao, Q., Zhang, Z., & Zhang, Z., (2020). Spatiotemporal variability of land surface albedo over the Tibet Plateau from 2001 to 2019. **Remote Sensing**, 12(7), 1188.

Liu, J., Worth, D., Desjardins, R., Haak, D., McConkey, B., & Cerkowniak, D., (2020). Influence of two management practices in the Canadian Prairies on radiative forcing. **Science of the Total Environment**, 142701.

Lone, B.A., Fayaz, A., Manzoor, M., Andrabi, N., Qayoom, S., Dar, Z., Rasool, F., Lone, A., Kumar, S., & Mushatq, N., (2020). An overview of climate change and its impact on crop productivity. **HISTORY**, p.2.

Maghrabi, A., & Al-Mostafa, Z., (2009). Estimating surface albedo over Saudi Arabia. **Renewable energy**, 34(6), 1607–1610.

Meng, C., (2020). Surface albedo assimilation and its impact Surface Radiation Budget in Beijing. **Advances in Meteorology**, 2020, 2020.

Oliveira, B. S., Moraes, E.C., Rudorff, B. F. T., & Mataveli, G. A. V., (2015). Análise do desempenho de modelos de albedo da superfície em áreas de cana-de-açúcar com dados do sensor MODIS/TERRA. **Revista Brasileira de Cartografia**, 67(3).

Psiloglou, B., Kambezidis, & H., (2009). Estimation of the ground albedo for the Athens area, Greece. **Journal of Atmospheric and Solar-Terrestrial Physics**, 71(8-9), 943–954.

Reis, R. P., Reis, A. J. D., Fontes, R. E., Takaki, H. R. C., & Castro Junior, L. G. D., (2001). Custos de produção da cafeicultura no sul de Minas Gerais.

Ridgwell, A., Singarayer, J. S., Hetherington, A. M., Valdes, P. J., (2009). Tackling regional climate change by leaf albedo bio-geoengineering. **Current Biology**, 19(2), 146–150.

Rodrigues, F., Von Pinho, R.G., FARIA FILHO, E.M., & GOULART, J.D.C., (2009). Capacidade de combinação entre linhagens de milho visando à produção de milho verde. **Bragantia**, 68, 75–84.

Sarafanov, M., Kazakov, E., Nikitin, N.O., & Kalyuzhnaya, A.V., (2020). A machine learning approach for remote sensing data gap-filling with open- source implementation: An example regarding land surface temperature, surface albedo and NDVI. **Remote Sensing**, 12(23), 3865.

Silva, E. C., & Maciel, G. M., (2010). Fluxo gênico em soja na região do sul de minas gerais. **Bioscience Journal**, 26(4).

Silva, S. D. M., Santos, A. C. D., & Lima, J. B. D., (2001). Competitividade do agronegócio do café na região sul de Minas Gerais.

Silva, B. B.; Lopes, G. M.; & de Azevedo, P.V., (2005). Determinação do albedo de áreas irrigadas com base em imagens Landsat 5-TM. **Revista Brasileira de Agrometeorologia**, 13(2), 11-21.

Spracklen, D. V., Bonn, B., & Carslaw, K. S., (2008). Boreal forests, aerosols and the impacts on clouds and climate. **Philosophical Transactions of the Royal Society A: Mathematical, Physical and Engineering Sciences**, 366(1885), 4613–4626.

Stein, M.L., (2012). Interpolation of spatial data: some theory for kriging. **Springer Science & Business Media**.

Wang, L., Zhang, D., Chen, C., Hu, F., & Zhang, L., (2020). Impact analysis of surface albedo heterogeneity on shortwave radiation using a 3D radiative transfer model. **Journal of Atmospheric and Solar-Terrestrial Physics**, 204, 105287.

Wang, Z., Schaaf, C. B., Sun, Q., Shuai, Y., & Román, M.O., (2018). Capturing rapid land surface dynamics with Collection V006 MODIS BRDF/NBAR/Albedo (MCD43) products. **Remote Sensing of Environment**, 207, 50–64.

Yin, X., 1998. The albedo of vegetated land surfaces: Systems Analysisand Mathematical Modeling. **Theoretical and applied climatology**, 60(1), 121–140.

Zhang, Y. F., Wang, X. P., Pan, Y. X., & Hu, R., (2013). Diurnal and seasonal variations of surface albedo in a spring wheat field of arid lands of Northwestern China. **International journal of Biometeorology**, 57(1), 67–73.

Zhou, M., Chen, G., Dong, Z., Xie, B., Gu, S., & Shi, P., (2020). Estimation of surface albedo from meteorological observations across China. **Agricultural and Forest Meteorology**, 281, 107848.

Zolotokrylin, A. N., Brito-Castillo, L., Titkova, T. B., (2020). Local climatically-driven changes of albedo and surface temperatures in the Sonoran Desert. **Journal of Arid Environments**, 178, 104147.